

Optimal Placement of Virtual Inertia in Power Grids

Bala Kameshwar Poolla Saverio Bolognani Florian Dörfler*

January 14, 2016

Abstract

A major transition in the operation of electric power grids is the replacement of bulk generation based on synchronous machines by distributed generation based on low-inertia power electronic sources. The accompanying “loss of rotational inertia” and the fluctuations by renewable sources jeopardize the system stability, as testified by the ever-growing number of frequency incidents. As a remedy, numerous studies demonstrate how virtual inertia can be emulated through various devices, but few of them address the question of “where” to place this inertia. It is however strongly believed that the placement of virtual inertia hugely impacts system efficiency, as demonstrated by recent case studies. In this article, we carry out a comprehensive analysis in an attempt to address the optimal inertia placement problem. We consider a linear network-reduced power system model along with an \mathcal{H}_2 performance metric accounting for the network coherency. The optimal inertia placement problem turns out to be non-convex, yet we provide a set of closed-form global optimality results for particular problem instances as well as a computational approach resulting in locally optimal solutions. We illustrate our results with a three-region power grid case study and compare our locally optimal solution with different placement heuristics in terms of different performance metrics.

1 Introduction

As we retire more and more synchronous machines and replace them by renewable sources interfaced with power electronic devices, the stability of the power grid is jeopardized, which has been recognized as one of the prime concerns by transmission system operators [1, 2]. Both in transmission grids as well as in microgrids, low inertia levels together with variable renewable generation lead to large frequency swings.

Not only are low levels of inertia troublesome, but particularly spatially heterogeneous and time-varying inertia profiles can lead to destabilizing effects, as shown in an interesting two-area case study [3]. It is not surprising that rotational inertia has been recognized as a key ancillary service for power system stability, and a plethora of mechanisms have been proposed for the emulation of virtual (or

synthetic) inertia [4–6] through a variety of devices (ranging from wind turbine control [7] over flywheels to batteries [8]), as well as inertia monitoring schemes [9] and even inertia markets [10]. In this article, we pursue the questions raised in [3] regarding the detrimental effects of spatially heterogeneous inertia profiles, and how they can be alleviated by virtual inertia emulation throughout the grid. In particular, we are interested in the allocation problem “where to optimally place the inertia” ?

The problem of inertia allocation has been hinted at before [3], but we are aware only of the study [11] explicitly addressing the problem. In [11], the grid is modeled by the linearized swing equations, and eigenvalue damping ratios as well as transient overshoots (estimated from the system modes) are chosen as optimization criteria for placing virtual inertia and damping. The resulting problem is highly non-convex, but a sequence of approximations led to some insightful results.

In comparison to [11], we focus on network coherency as an alternative performance metric, that is, the amplification of stochastic or impulsive disturbances via a quadratic performance index measured by the \mathcal{H}_2 norm [12]. As performance index, we choose a classic coherency criterion penalizing angular differences and absolute frequencies, which has recently been popularized for consensus and synchronization studies [13–18] as well as in power system analysis and control [19–21]. We feel that this \mathcal{H}_2 performance metric is not only more tractable than spectral metrics, but it is also very meaningful for the problem at hand: it measures the effect of stochastic fluctuations (caused by loads and/or variable renewable generation) as well as impulsive events (such as faults or deterministic frequency errors caused by markets) and quantifies their amplification by a coherency index directly related to frequency volatility. Finally, in comparison to [11], the damping or droop coefficients are not decision variables in our problem setup, since these are determined by the system physics (in case of damping), the outcome of primary reserve markets (in case of primary control), or scheduled according to cost coefficients, ratings, or grid-code requirements [22].

The contributions of this paper are as follows. We provide a comprehensive modeling and analysis framework for the inertia placement problem in power grids to optimize an \mathcal{H}_2 coherency index subject to capacity and budget constraints. The optimal inertia placement problem is characteristically non-convex, yet we are able to provide explicit upper and lower bounds on the performance index. Additionally, we show that the problem admits an elegant and strictly convex

*This material is supported by ETH start-up funds and the SNF Assistant Professor Energy Grant #160573. B.K. Poolla, S. Bolognani, and F. Dörfler are with the Automatic Control Laboratory at the Swiss Federal Institute of Technology (ETH) Zürich, Switzerland. Emails: {bpoolla, bsaverio, dorfler}@ethz.ch.

reformulation for a performance index reflecting the cost of primary control which is often advocated as a remedy to low-inertia stability issues. In this case, the optimal inertia placement problem reduces to a standard resource allocation problem, where the cost of each resource is proportional to the ratio of expected disturbance over inertia.

A similar simplification of the problem is obtained under some reasonable assumptions on the ratio between the disturbance and the damping coefficient at every node. For the case of a two-area network, a closed-form global allocation is derived, and a series of observations are discussed.

Furthermore, we develop a computational approach based on a gradient formula that allows us to find a locally optimal solution for large networks and arbitrary parameters. We show how the combinatorial problem of allocating a limited number of inertia-emulating units can be also incorporated into this numerical method via a sparsity-promoting approach.

A detailed three-region network has been adopted as case study for the presentation of the proposed method. The numerical results are also illustrated via time-domain simulations, that demonstrate how an optimization-based allocation exhibits superior performance (in different performance metrics) compared to heuristic placements, and, perhaps surprisingly, the optimal allocation also uses less effort to emulate inertia.

From the methodological point of view, this paper extends the \mathcal{H}_2 performance analysis of second-order consensus systems to non-uniform damping, inertia, and input matrices (disturbance location). This technical contribution is essential for the application that we are considering, as these parameters dictate the optimal inertia allocation in an intertwined way.

The remainder of this section introduces some notation. Section 2 motivates our system model and the coherency performance index. Section 3 presents numerical inertia allocation algorithms for general networks and provides explicit results for certain instances of cost functions and problem scenarios. Section 4 presents a case study on a three-region network accompanied with time-domain simulations and a spectral analysis. Finally, Section 5 concludes the paper.

Notation We denote the n -dimensional vectors of all ones and zeros by $\mathbf{1}_n$ and $\mathbf{0}_n$. Given an index set \mathcal{I} with cardinality $|\mathcal{I}|$ and a real-valued array $\{x_1 \dots x_{|\mathcal{I}|}\}$, we denote by $x \in \mathbb{R}^{|\mathcal{I}|}$ the vector obtained by stacking the scalars x_i and by $\text{diag}\{x_i\}$ the associated diagonal matrix. The vector e_i is the i -th vector of the canonical basis for \mathbb{R}^n .

2 Problem Formulation

2.1 System model

Consider a power network modeled by a graph with nodes (buses) $\mathcal{V} = \{1, \dots, n\}$ and edges (transmission lines) $\mathcal{E} \subseteq \mathcal{V} \times \mathcal{V}$. We consider a small-signal version of a network-reduced power system model [23, 24], where passive loads

are eliminated via Kron reduction [25], and the network is reduced to the sources $i \in \{1, \dots, n\}$ with dynamics

$$m_i \ddot{\theta}_i + d_i \dot{\theta}_i = p_{\text{in},i} - p_{e,i}, \quad i \in \{1, \dots, n\}, \quad (1)$$

where $p_{\text{in},i}$ and $p_{e,i}$ refer to the power input and electrical power output, respectively. If bus i is a synchronous machine, then (1) describes the electromechanical swing dynamics for the generator rotor angle θ_i [23, 24], $m_i > 0$ is the generator's rotational inertia, and $d_i > 0$ accounts for frequency damping or speed droop control (neglecting ramping limits). If bus i connects to a renewable or battery source interfaced with a power electronics inverter operated in grid-forming mode [26, 27], then θ_i is the voltage phase angle, $d_i > 0$ is the droop control coefficient, and $m_i > 0$ accounts for power measurement time constant [28] or arises from virtual inertia emulation through a dedicated controlled device [4–6]. Finally, the dynamics (1) may also arise from frequency-dependent or actively controlled frequency-responsive loads [24].

Under the assumptions of constant voltage magnitudes, purely inductive lines, and a small signal approximation, the electrical power output at the terminals is given by [24]

$$p_{e,i} = \sum_{j=1}^n b_{ij}(\theta_i - \theta_j), \quad i \in \{1, \dots, n\}, \quad (2)$$

where $b_{ij} \geq 0$ is the susceptance between nodes $\{i, j\} \in \mathcal{E}$.

The state space representation of the system (1)-(2) is then

$$\begin{bmatrix} \dot{\theta} \\ \dot{\omega} \end{bmatrix} = \begin{bmatrix} 0 & I \\ -M^{-1}L & -M^{-1}D \end{bmatrix} \begin{bmatrix} \theta \\ \omega \end{bmatrix} + \begin{bmatrix} 0 \\ M^{-1} \end{bmatrix} p_{\text{in}}, \quad (3)$$

where $M = \text{diag}\{m_i\}$ and $D = \text{diag}\{d_i\}$ are the diagonal matrices of inertial and damping/droop coefficients, and $L = L^T \in \mathbb{R}^{n \times n}$ is the network Laplacian (or susceptance) matrix with off-diagonal elements $l_{ij} = -b_{ij}$ and diagonals $l_{ii} = \sum_{j=1, j \neq i}^n b_{ij}$. The states $(\theta, \omega) \in \mathbb{R}^{2n}$ are the stacked vectors of angles and frequencies and $p_{\text{in}} \in \mathbb{R}^n$ is the net power input – all of which are deviation variables from nominal values.

2.2 Coherency performance metric

We consider the linear power system model (3) driven by the inputs $p_{\text{in},i}$ accounting either for faults or non-zero initial values (modeled as impulses) or for random fluctuations in renewables and loads. We are interested in the energy expended in returning to the steady-state configuration, expressed as a quadratic cost of the angle differences and frequency displacements:

$$\int_0^\infty \sum_{i,j=1}^n a_{ij}(\theta_i(t) - \theta_j(t))^2 + \sum_{i=1}^n s_i \omega_i^2(t) dt. \quad (4)$$

Here, s_i are positive scalars and we assume that the nonnegative scalars $a_{ij} = a_{ji} \geq 0$ induce a connected graph – not necessarily identical with the power grid itself. We denote by S the matrix $\text{diag}\{s_i\}$, and by N the Laplacian matrix of the graph induced by the a_{ij} . In this compact notation, $N = L$ would be an example of short-range error penalization [13, 14], while $N = I_n - \mathbf{1}_n \mathbf{1}_n^T / n$ penalizes long-range errors.

Aside from consensus and synchronization studies [13–18] the coherency metric (4) has recently also been used in power system analysis and control [19–21]. Following the interpretation proposed in [19], the above metric (4) can represent a generalized energy in synchronous machines. Indeed, for $a_{ij} = g_{ij}$ (where g_{ij} are the power line conductances) and $s_i = m_i$, the metric (4) accounts for the heat losses in the grid lines and the mechanical energy losses in the generators.

Adopting the state representation introduced in (3), the performance metric (4) can be rewritten as the time-integral $\int_0^\infty y(t)^\top y(t) dt$ of the performance output

$$y = \underbrace{\begin{bmatrix} N^{\frac{1}{2}} & 0 \\ 0 & S^{\frac{1}{2}} \end{bmatrix}}_{=C} \begin{bmatrix} \theta \\ \omega \end{bmatrix}. \quad (5)$$

In order to model the localization of the disturbances in the grid, we parametrize the input p_{in} as

$$p_{\text{in}} = T^{\frac{1}{2}} \eta, \quad T = \text{diag}\{t_i\}, \quad t_i \geq 0$$

We therefore obtain the state space model

$$\begin{bmatrix} \dot{\theta} \\ \dot{\omega} \end{bmatrix} = \underbrace{\begin{bmatrix} 0 & I \\ -M^{-1}L & -M^{-1}D \end{bmatrix}}_{=A} \begin{bmatrix} \theta \\ \omega \end{bmatrix} + \underbrace{\begin{bmatrix} 0 \\ M^{-1}T^{1/2} \end{bmatrix}}_{=B} \eta. \quad (6)$$

In the following, we refer to the input/output map (5), (6) as $G = (A, B, C)$. If the inputs η_i are Dirac impulses, then (4) measures the squared \mathcal{H}_2 norm $\|G\|_2$ of the system [12].

There is a number of interpretations of the \mathcal{H}_2 norm $\|G\|_2$ of a power system [19]. The relevant ones in our context are:

1. The squared \mathcal{H}_2 norm of G measures the energy amplification, i.e., the sum of \mathcal{L}_2 norms of the outputs $y_i(t)$, for unit impulses at all inputs $\eta_i(t) = \delta(t)$:

$$\|G\|_2^2 = \sum_{i=1}^n \int_0^\infty y_i^\top(t) y_i(t) dt.$$

These impulses can model faults or initial conditions.

2. The squared \mathcal{H}_2 norm of G quantifies the steady-state total variance of the output for a system subjected to unit variance stochastic white noise inputs $\eta_i(t)$:

$$\|G\|_2^2 = \lim_{t \rightarrow \infty} E \{ y^\top(t) y(t) \}.$$

In our case, the white noise inputs can model stochastic fluctuations of renewable generation or loads.

In general, the \mathcal{H}_2 norm of a linear system can be calculated efficiently by solving a linear Lyapunov equation. In our case an additional linear constraint is needed to account for the marginally stable and undetectable mode $v_0 = [\mathbf{1}_n^\top \mathbf{0}_n^\top]^\top$ corresponding to an absolute angle reference for the grid.

Lemma 1. (\mathcal{H}_2 norm via observability Gramian) *For the state-space system (A, B, C) defined above, we have that*

$$\|G\|_2^2 = \text{Trace}(B^\top P B), \quad (7)$$

where the observability Gramian $P \in \mathbb{R}^{2n \times 2n}$ is uniquely defined by the following Lyapunov equation and an additional constraint defined by $v_0 = [\mathbf{1}_n^\top \mathbf{0}_n^\top]^\top$:

$$PA + A^\top P + C^\top C = 0, \quad (8)$$

$$P v_0 = \mathbf{0}_{2n}. \quad (9)$$

Proof. Following the typical derivation of the \mathcal{H}_2 norm for state-space systems [12], we have $\|G\|_2^2 = \text{Trace}(B^\top \hat{P} B)$, where \hat{P} is the observability Gramian $\hat{P} = \int_0^\infty e^{A^\top t} C^\top C e^{A t} dt$. Note from (5) that the mode $v_0 = [\mathbf{1}_n^\top \mathbf{0}_n^\top]^\top$ associated with the marginally stable eigenvalue of A is not detectable, i.e., it holds that $C e^{A t} v_0 = C v_0 = \mathbf{0}_{2n}$ for all $t \geq 0$. Because the remaining eigenvalues of A are stable, the indefinite integral exists.

Next, we show that \hat{P} is a solution for both (8) and (9). By taking the derivative of $e^{A^\top t} C^\top C e^{A t}$ with respect to t , and then by integrating from $t = 0$ to $t = +\infty$, we obtain

$$A^\top \hat{P} + \hat{P} A = \left[e^{A^\top t} C^\top C e^{A t} \right]_0^\infty.$$

Using the fact that $C v_0 = A v_0 = \mathbf{0}_{2n}$, we conclude that $\left[e^{A^\top t} C^\top C e^{A t} \right]_0^\infty = -C^\top C$ and therefore (8) holds for \hat{P} . The fact that \hat{P} satisfies (9) can be verified by inspection, as

$$\hat{P} v_0 = \int_0^\infty e^{A^\top t} C^\top C e^{A t} v_0 dt = \int_0^\infty e^{A^\top t} C^\top C v_0 dt = \mathbf{0}_{2n}.$$

It remains to show that the \hat{P} is the unique solution of (8) and (9). To this end, note that $\text{rank}(A^\top) = 2n - 1$ and the rank-nullity theorem imply that the kernel of A^\top is given by a vector $\xi \in \mathbb{R}^{2n}$. It can be verified that $A^\top \xi = \mathbf{0}_{2n}$ holds for $\xi = [(D \mathbf{1}_n)^\top (M \mathbf{1}_n)^\top]^\top$, and it directly follows that all solutions of (8) are parametrized by

$$P(\tau) = \hat{P} + \tau \xi \xi^\top,$$

for $\tau \in \mathbb{R}$. Finally, (9) holds if $(\hat{P} + \tau \xi \xi^\top) v_0 = \mathbf{0}_{2n}$. In combination with $\hat{P} v_0 = \mathbf{0}_{2n}$ this implies $\tau = 0$. With this choice of τ , P equals the positive semidefinite matrix \hat{P} . \square

3 Optimal inertia allocation

We assume that each node $i \in \{1, \dots, n\}$ has a nonzero¹ inertial coefficient $\underline{m}_i > 0$ and we are interested in optimally allocating additional virtual inertia in order to minimize the \mathcal{H}_2 norm (4), subject to upper bounds \overline{m}_i at each bus, and a total budget constraint m_{bdg} , accounting for the available installation space and the total cost of the storage devices.

This problem statement is summarized as

$$\underset{P, m_i}{\text{minimize}} \quad \|G\|_2^2 = \text{Trace}(B^\top P B) \quad (10a)$$

$$\text{subject to} \quad \sum_{i=1}^n m_i \leq m_{\text{bdg}} \quad (10b)$$

$$\underline{m}_i \leq m_i \leq \overline{m}_i, \quad i \in \{1, \dots, n\} \quad (10c)$$

$$PA + A^\top P + C^\top C = 0, \quad P v_0 = \mathbf{0}_{2n}, \quad (10d)$$

¹Observe that the case $m_i = 0$ leads to an ill-posed model (1) whose number of algebraic and dynamic states depend on the system parameters.

where (A, B, C) are the matrices of the input-output system (5)-(6). Observe the bilinear nature of the Lyapunov constraint (10d) featuring products of A and P , and recall from (6) that the decision variables m_i appear as m_i^{-1} in A . Hence, the problem (10) is highly non-convex and typically also large-scale.

In the following, we will provide general lower and upper bounds, a simplified formulation under certain parametric assumptions, a detailed analysis of a two-area power system, and a numerical method determine locally optimal solutions in the fully general case.

3.1 Performance bounds

Theorem 2. (Performance bounds) *Consider the power system model (5)-(6), the squared \mathcal{H}_2 norm (7), and the optimal inertia allocation problem (10). Then the objective (10a) satisfies*

$$\begin{aligned} & \frac{\underline{t}}{2\bar{d}} \left(\text{Trace}(NL^\dagger) + \sum_{i=1}^n \frac{s_i}{m_i} \right) \\ & \leq \|G\|_2^2 \leq \frac{\bar{t}}{2\underline{d}} \left(\text{Trace}(NL^\dagger) + \sum_{i=1}^n \frac{s_i}{m_i} \right), \end{aligned} \quad (11)$$

where $\underline{t} = \min_i \{t_i\}$, $\bar{t} = \max_i \{t_i\}$, $\underline{d} = \min_i \{d_i\}$, and $\bar{d} = \max_i \{d_i\}$.

Proof. Let us express the observability Gramian P as the block matrix

$$P = \begin{bmatrix} X_1 & X_0 \\ X_0^\top & X_2 \end{bmatrix}.$$

With this notation, the squared \mathcal{H}_2 norm (7), $\|G\|_2^2$ reads as

$$\text{Trace}(B^\top P B) = \text{Trace}(T M^{-2} X_2) = \sum_{i=1}^n \frac{t_i X_{2,ii}}{m_i^2}, \quad (12)$$

where we used the ring commutativity of the trace and the fact that $T^{1/2}$ and M^{-1} are diagonal and therefore commute.

The constraint (10d) can be expanded as

$$\begin{bmatrix} X_1 & X_0 \\ X_0^\top & X_2 \end{bmatrix} A + A^\top \begin{bmatrix} X_1 & X_0 \\ X_0^\top & X_2 \end{bmatrix} + \begin{bmatrix} N & 0 \\ 0 & S \end{bmatrix} = 0. \quad (13)$$

By right-multiplying the (1,1) equation of (13) by the Moore-Penrose pseudo-inverse L^\dagger of the Laplacian L , we obtain

$$-X_0 M^{-1} L L^\dagger - L M^{-1} X_0^\top L^\dagger = -N L^\dagger.$$

By the constraint (9) we have that $[\mathbf{1}_n^\top \ 0_n^\top] P = [0_n^\top \ 0_n^\top]$ which implies $\mathbf{1}_n^\top X_0 = 0_n^\top$. This fact together with the identity $L L^\dagger = (I_n - \mathbf{1}_n \mathbf{1}_n^\top / n)$, implies that $L L^\dagger X_0 = X_0$. Then, by using the ring commutativity of the trace, and its invariance with respect to transposition of the argument, we obtain

$$2 \text{Trace}(M^{-1} X_0) = \text{Trace}(N L^\dagger). \quad (14)$$

On the other hand, equation (2,2) of (13) implies that

$$X_0^\top + X_0 = X_2 M^{-1} D + D M^{-1} X_2 - S.$$

Similarly as before we left-multiply by M^{-1} , use trace properties and the commutativity of M^{-1} and D , and obtain

$$2 \text{Trace}(M^{-1} X_0 - D M^{-2} X_2) = -\text{Trace}(M^{-1} S). \quad (15)$$

Thus, (14) and (15) together deliver

$$\text{Trace}(D M^{-2} X_2) = \frac{1}{2} \text{Trace}(M^{-1} S + N L^\dagger). \quad (16)$$

From (12) we obtain the relations

$$\underline{t} \sum_{i=1}^n \frac{X_{2,ii}}{m_i^2} \leq \|G\|_2^2 \leq \bar{t} \sum_{i=1}^n \frac{X_{2,ii}}{m_i^2},$$

which can be further bounded as

$$\frac{\underline{t}}{\underline{d}} \sum_{i=1}^n \frac{d_i X_{2,ii}}{m_i^2} \leq \|G\|_2^2 \leq \frac{\bar{t}}{\bar{d}} \sum_{i=1}^n \frac{d_i X_{2,ii}}{m_i^2}. \quad (17)$$

The structural similarity of (16) and (17) allows us to state upper and lower bounds by rewriting (17) as in (11). \square

Notice that in the bounds proposed in Theorem 2, the network topology described by the Laplacian L enters only as a constant factor, and is decoupled from the decision variables m_i . Moreover, in the case $N = L$ (short-range error penalty on angles differences), this offset term becomes just a function of the grid size: $\text{Trace}(N L^\dagger) = \text{Trace}(L L^\dagger) = n - 1$.

Theorem 2 (and its proof) sheds some light on the nature of the optimization problem that we are considering, and in particular on the role played by the mutual relation between disturbance strengths t_i , damping coefficients d_i , their ratios t_i/d_i , frequency penalty weights s_i , and the decision variables m_i . These insights are further developed in the next section.

3.2 Noteworthy cases

In this section, we consider some special choices of the performance metric and some assumptions on the system parameters, which are practically relevant and yield simplified versions of the general optimization problem (10), enabling in most cases the derivation of closed-form solutions.

We first consider the performance index (4) corresponding to the cost of primary control. As a remedy to mitigate low-inertia frequency stability issues, additional fast-ramping primary control is often put forward [3]. The primary control effort can be accounted for by the integral quadratic cost

$$\int_0^\infty \dot{\theta}(t)^\top D \dot{\theta}(t) dt. \quad (18)$$

Hence, the cost of primary control (18) mimics the \mathcal{H}_2 performance where the performance matrices in (5) are chosen as $N = 0$ and $S = D$. This intuitive cost functions allows an insightful simplification of the optimization problem (10).

Theorem 3. (Primary control cost minimization)

Consider the power system model (5)-(6), the squared \mathcal{H}_2 norm (7), and the optimal inertia allocation problem (10). For a performance output characterizing the cost of primary

control (18): $S = D$ and $N = 0$, the optimization problem (10) can be equivalently restated as the convex problem

$$\underset{m_i}{\text{minimize}} \quad \sum_{i=1}^n \frac{t_i}{m_i} \quad (19a)$$

$$\text{subject to} \quad \sum_{i=1}^n m_i \leq m_{\text{bdg}} \quad (19b)$$

$$\underline{m}_i \leq m_i \leq \overline{m}_i, \quad i \in \{1, \dots, n\}, \quad (19c)$$

where, we recall, t_i describes the strength of the disturbance at node i .

Proof. With $N = 0$ and $S = D$, the Lyapunov equation (13) together with the constraint (9) is solved explicitly by

$$P = \begin{bmatrix} X_1 & X_0 \\ X_0^\top & X_2 \end{bmatrix} = \frac{1}{2} \begin{bmatrix} L & 0 \\ 0 & M \end{bmatrix}.$$

The performance metric as derived in (12) therefore becomes

$$\|G\|_2^2 = \sum_{i=1}^n \frac{t_i X_{2,ii}}{m_i^2} = \frac{1}{2} \sum_{i=1}^n \frac{t_i}{m_i}.$$

This concludes the proof. \square

The equivalent convex formulation (19) yields the following important insights. First and foremost, the optimal solution to (19) is unique (as long as at least one t_i is greater than zero) and also independent of the network topology and the line susceptances. It depends solely on the location and strength of the disturbance as encoded in the coefficients t_i . For example, if the disturbance is concentrated at a particular node i with $t_i \neq 0$ and $t_j = 0$ for $j \neq i$, then the optimal solution is to allocate the maximal inertia at node i : $m_i = \min\{m_{\text{bdg}}, \overline{m}_i\}$. In absence of capacity constraints (19c) and presence of the budget constraint (19b), the optimal inertia allocation is proportional to the square root of the disturbance $\sqrt{t_i}$.

We now consider a different assumption that also allows to derive a similar simplified analysis in other notable cases.

Assumption 1. (Uniform disturbance-damping ratio) *The ratio $\lambda = t_i/d_i$ is constant for all $i \in \{1, \dots, n\}$.* \square

Notice that the droop coefficients d_i are often scheduled proportionally to the rating of a power source, to guarantee fair power sharing [22]. Meanwhile, it is reasonable to expect that the disturbances due to variable renewable fluctuations scale proportionally to the size of the renewable power source. Hence, Assumption 1 can be justified in many practical cases, including of course the case where both damping coefficient and disturbances are uniform across the grid. Under this assumption, we have the following result.

Theorem 4. (Optimal allocation with uniform disturbance-damping ratio) *Consider the power system model (5)-(6), the squared \mathcal{H}_2 norm (7), and the optimal inertia allocation problem (10). Let Assumption 1 hold. Then*

the optimization problem (10) can be equivalently restated as the convex problem

$$\underset{m_i}{\text{minimize}} \quad \sum_{i=1}^n \frac{s_i}{m_i} \quad (20a)$$

$$\text{subject to} \quad \sum_{i=1}^n m_i \leq m_{\text{bdg}} \quad (20b)$$

$$\underline{m}_i \leq m_i \leq \overline{m}_i, \quad i \in \{1, \dots, n\}, \quad (20c)$$

where we recall that s_i is the penalty coefficient for the frequency deviation at node i .

Proof. From Assumption 1, let $\lambda = t_i/d_i > 0$ be constant for all $i \in \{1, \dots, n\}$. Then we can rewrite (12) as

$$\|G\|_2^2 = \sum_{i=1}^n \frac{t_i X_{2,ii}}{m_i^2} = \lambda \sum_{i=1}^n \frac{d_i X_{2,ii}}{m_i^2}.$$

This is equal, up to the scaling factor λ , to the left hand side of (16). We therefore have

$$\|G\|_2^2 = \frac{\lambda}{2} \text{Trace}(M^{-1}S + NL^\dagger), \quad (21)$$

which is equivalent, up to multiplicative factors and constant offsets, to the cost of the optimization problem (20a). \square

Again, as in Theorem 3, Theorem 4 reduces the original optimization problem to a simple convex problem for which the optimal inertia allocation is *independent* of the network topology, and in most cases can be derived as a closed form expression of the problem parameters.

Under Assumption 1, we can also identify an interesting special case. Assume that the frequency penalty S is chosen proportional to inertia coefficients, $S = cM$ for some $c \geq 0$:

$$\int_0^\infty \sum_{i,j=1}^n a_{ij} (\theta_i(t) - \theta_j(t))^2 + c \cdot \sum_{i=1}^n m_i \omega_i^2(t) dt.$$

This choice corresponds to penalizing the change in kinetic energy – a reasonable and standard penalty in power systems. We have the subsequent result, that follows directly by evaluating (21) for this specific choice of $S = c \cdot M$ (which also includes the case where no frequency penalty is considered, i.e. $c = 0$, and therefore only angle differences are penalized).

Corollary 5. (Kinetic energy penalization with uniform disturbance-damping ratio) *Let Assumption 1 hold, and let the penalty on the frequency deviations be proportional to the allocated inertia, that is, $S = c \cdot M$. Then the performance metric $\|G\|_2^2$ is independent on the inertia allocation, and assumes the form*

$$\|G\|_2^2 = \frac{\lambda}{2} (c \cdot n + \text{Trace}(NL^\dagger)),$$

where $\lambda = t_i/d_i > 0$, for all $i \in \{1, \dots, n\}$, is the uniform disturbance-damping ratio.

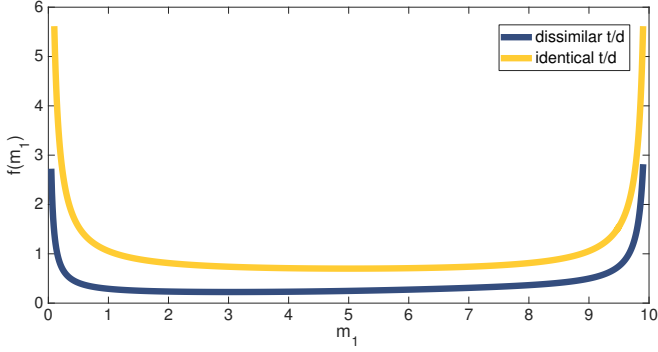


Figure 1: Cost function profiles for identical and weakly dissimilar t_i/d_i ratios for the two-area case.

3.3 Explicit results for a two-area network

In this subsection, we focus on a two-area power grid as in [3] to obtain some insight on the nature of this optimization problem. We also highlight the role of the ratios t_i/d_i , which play a prominent role in Assumption 1 and the bounds (11).

In the case of a two-area system, it is possible to derive an analytical solution $P(m)$ of the Lyapunov equation (10d), as a closed form function of the vector of inertia allocations m_i . We thus obtain an explicit expression for the objective (10a) as

$$\|G\|_2^2 = f(m) := \text{Trace}(B(m)^\top P(m)B(m)) \quad (22)$$

where $f(m)$ is a rational function of polynomials of orders 4 in the numerator (respectively, 6 in the denominator) in terms of inertial coefficients m_i .

As the explicit expression is more convoluted than insightful, we will not show it here, but only report the following statements which can be verified by a simple but cumbersome analysis of the rational function $f(m)$:

1. The problem (10) admits a unique minimizer.
2. For sufficiently large bounds \bar{m}_i , the budget constraint (10b) becomes active, that is, the optimizers satisfy $m_1^* + m_2^* = m_{\text{bdg}}$. In this case, m_2 can be eliminated as $m_2 = m_{\text{bdg}} - m_1$, and (10) can be reduced to a scalar problem.
3. In case of no capacity constraints and for identical t_i/d_i ratios and frequency penalties S , the optimal inertial coefficients are identical $m_1^* = m_2^*$ (as predicted by Theorem 4). In case that $t_i/d_i > t_j/d_j$, then $m_i^* > m_j^*$ (see the example in Figure 1, where we eliminated $m_2^* = m_{\text{bdg}} - m_1^*$).
4. For sufficiently uniform t_i/d_i ratios, the problem (10) is strongly convex. We observe that the cost function $f(m)$ is fairly flat over the feasible set (see Figure 1).
5. For strongly dissimilar t_i/d_i ratios, we observe a less flat cost function. If the disturbance affects only one node, for example, $t_1 = 1$ and $t_2 = 0$, strong convexity is lost.

From the above facts, we conclude that the input scaling factors t_i play a fundamental role in the determination of the optimal inertia allocation. To obtain a more complete

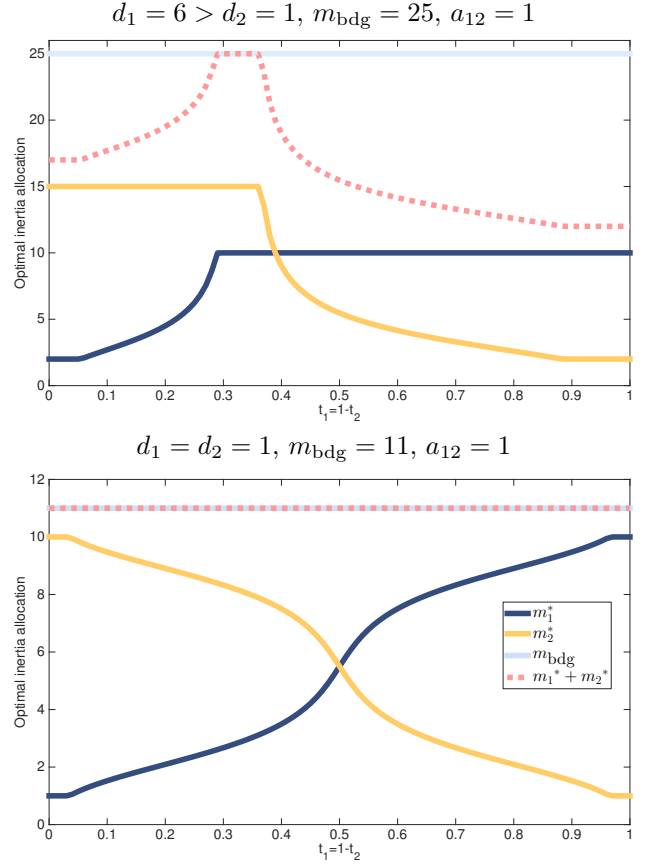


Figure 2: Optimal inertia allocation for a two-area system with identical frequency penalties $S = I_2$, with non-identical and identical damping coefficients d_i , with disturbance inputs varying from $[t_1, t_2] = [0, 1]$ to $[t_1, t_2] = [1, 0]$, and for two choices of budget m_{bdg} .

picture, we linearly vary the disturbance input matrices from $[t_1, t_2] = [0, 1]$ to $[t_1, t_2] = [1, 0]$, that is, from a disturbance localized at node 2 to a disturbance localized at node 1. The resulting optimizers are displayed in Figure 2 showing that inertia is allocated dominantly at the site of the disturbance, which is in line with previous case studies [3, 11]. Notice also that depending on the value of the budget m_{bdg} , the capacity constraints \bar{m}_i , and the t_i/d_i ratios, the budget constraint may be active or not. Thus, perhaps surprisingly, sometimes not all inertia resources are allocated. Overall, the two-area case paints a surprisingly complex picture.

3.4 A numerical method for the general case

In Subsections 3.2 and 3.3, we considered a subset of scenarios and cost functions that allowed the derivation of tractable reformulations and solutions of the inertia allocation problem (10). In this section, we consider the optimization problem in its full generality. Similarly as in Section 3.3, we denote by $P(m)$ the solution to the Lyapunov equation (10d), and we express the cost function $\|G\|_2^2$ as a function $f(m)$ of the vector of inertia allocations m_i , i.e.

$$\|G\|_2^2 = f(m) := \text{Trace}(B(m)^\top P(m)B(m)). \quad (23)$$

The proposed computational approach consists of deriving an efficient algorithm for the computation of the gradient $\nabla f(m)$ of $f(m)$. Information on the gradient $\nabla f(m)$ is essential for many numerical optimization methods, for example, the problem (10) can be approached via the *partial* Lagrangian

$$L(m, \bar{\rho}, \underline{\rho}, \varsigma) = f(m) + \bar{\rho}^\top (m - \bar{m}) + \underline{\rho}^\top (\underline{m} - m) + \varsigma \left(\sum_{i=1}^n m_i - m_{\text{bdg}} \right),$$

where $\bar{\rho}, \underline{\rho}, \varsigma > 0$ are multipliers, and we do not dualize the Lyapunov constraint (10d). If the gradient of $f(m)$ is explicitly available, then a locally optimal solution can be computed, for example, via the iterative primal-dual algorithm [29]

$$\begin{aligned} m(k+1) &= m(k) \\ &\quad - \alpha(k) (\nabla f(m(k)) + \bar{\rho}(k) - \underline{\rho}(k) + \varsigma(k) \mathbf{1}_n), \\ \bar{\rho}(k+1) &= [\bar{\rho}(k) + \alpha(k) (m(k) - \bar{m})]_+, \\ \underline{\rho}(k+1) &= [\underline{\rho}(k) + \alpha(k) (\underline{m} - m(k))]_+, \\ \varsigma(k+1) &= \left[\varsigma(k) + \alpha(k) \left(\sum_{i=1}^n m_i(k) - m_{\text{bdg}} \right) \right]_+, \end{aligned}$$

where $k \in \mathbb{Z}_{\geq 0}$ is the iteration index, $\alpha(k) > 0$ is an appropriate step size, and $[\cdot]_+ = \max\{0, \cdot\}$. In general, most computational approaches can be sped up tremendously if the large-scale set of nonlinear (in the decision variables) Lyapunov equations (10d) can be eliminated and included into the gradient information, as we are proposing. In the following, we provide an algorithm that achieves so using the routine **Lyap**(A, Q), which returns the matrix P that solves $PA + A^\top P + Q = 0$ together with $Pv_0 = 0_{2n}$.

Algorithm 1: Gradient computation

Input current value m of the decision variables

Output numerical evaluation g of the gradient $\nabla f(m)$

$$\begin{aligned} A^{(0)} &\leftarrow \begin{bmatrix} 0 & I \\ -M^{-1}L & -M^{-1}D \end{bmatrix}; \\ B^{(0)} &\leftarrow \begin{bmatrix} 0 \\ M^{-1}T^{1/2} \end{bmatrix}; \\ P^{(0)} &\leftarrow \mathbf{Lyap}(A^{(0)}, C^\top C); \\ \mathbf{for} \ i = 1, \dots, n \ \mathbf{do} & \\ \quad \Phi &\leftarrow e_i e_i^\top; \\ \quad A^{(1)} &\leftarrow \begin{bmatrix} 0 & 0 \\ \Phi M^{-2}L & \Phi M^{-2}D \end{bmatrix}; \\ \quad B^{(1)} &\leftarrow \begin{bmatrix} 0 \\ -\Phi M^{-2}T^{1/2} \end{bmatrix}; \\ \quad P^{(1)} &\leftarrow \mathbf{Lyap}(A^{(0)}, P^{(0)}A^{(1)} + A^{(1)\top}P^{(0)}); \\ \quad g_i &\leftarrow \mathbf{Trace}(2B^{(1)\top}P^{(0)}B^{(0)} + B^{(0)\top}P^{(1)}B^{(0)}); \end{aligned}$$

Theorem 6. (Gradient computation) Consider the objective function (23), where $P(m)$ is a function of m via the Lyapunov equation (10d). The objective function is differentiable for $m \in \mathbb{R}_{>0}^n$, and its gradient at m is given by Algorithm 1.

The proof of Theorem 6 is partially inspired by [16] and relies on a perturbation analysis of the Lyapunov equation (10d) combined with Taylor and power series expansions.

Proof. In order to compute the gradient of (23) at $m \in \mathbb{R}_{>0}^n$, we make use of the relation

$$\nabla_\mu f(m) = \nabla f(m)^\top \mu, \quad (24)$$

where $\nabla_\mu f(m)$ is the directional derivative of f in the direction $\mu \in \mathbb{R}^n$, defined as

$$\nabla_\mu f(m) = \lim_{\delta \rightarrow 0} \frac{f(m + \delta\mu) - f(m)}{\delta}, \quad (25)$$

whenever this limit exists. From (23) we have that

$$f(m + \delta\mu) = \text{Trace}(B(m + \delta\mu)^\top P B(m + \delta\mu)), \quad (26)$$

where P is a solution of the Lyapunov equation

$$PA(m + \delta\mu) + A(m + \delta\mu)^\top P + C^\top C = 0 \quad (27)$$

and where by $A(m + \delta\mu)$ we denote the system matrix defined in (6), evaluated at $m + \delta\mu$. The matrices $A(m + \delta\mu)$ and $B(m + \delta\mu)$ viewed as functions of scalar δ can thus be expanded in a Taylor series around $\delta = 0$ as

$$\begin{aligned} A(m + \delta\mu) &= A_{(m,\mu)}^{(0)} + A_{(m,\mu)}^{(1)}\delta + \mathcal{O}(\delta^2), \\ B(m + \delta\mu) &= B_{(m,\mu)}^{(0)} + B_{(m,\mu)}^{(1)}\delta + \mathcal{O}(\delta^2) \end{aligned} \quad (28)$$

with coefficients $A_{(m,\mu)}^{(i)}$ and $B_{(m,\mu)}^{(i)}$, $i \in \{0, 1\}$. To compute the coefficients of the Taylor expansion in (28), we recall the scalar series expansion of $1/(m_i + \delta\mu_i)$ around $\delta = 0$:

$$\frac{1}{(m_i + \delta\mu_i)} = \frac{1}{m_i} - \frac{\delta\mu_i}{m_i^2} + \mathcal{O}(\delta^2).$$

Using the shorthand $\Phi = \text{diag}(\mu_i)$, we therefore have

$$\begin{aligned} A_{(m,\mu)}^{(0)} &= \begin{bmatrix} 0 & I \\ -M^{-1}L & -M^{-1}D \end{bmatrix} \\ A_{(m,\mu)}^{(1)} &= \begin{bmatrix} 0 & 0 \\ \Phi M^{-2}L & \Phi M^{-2}D \end{bmatrix} \\ B_{(m,\mu)}^{(0)} &= \begin{bmatrix} 0 \\ M^{-1}T^{1/2} \end{bmatrix} \\ B_{(m,\mu)}^{(1)} &= \begin{bmatrix} 0 \\ -\Phi M^{-2}T^{1/2} \end{bmatrix}. \end{aligned}$$

Accordingly, the solution to the Lyapunov equation (27) can be expanded in a power series as

$$P = P(m + \delta\mu) = P_{(m,\mu)}^{(0)} + P_{(m,\mu)}^{(1)}\delta + \mathcal{O}(\delta^2), \quad (29)$$

and therefore the Lyapunov equation (27) becomes

$$\begin{aligned} (P^{(0)} + \delta P^{(1)} + \mathcal{O}(\delta^2))(A^{(0)} + \delta A^{(1)} + \mathcal{O}(\delta^2)) + \\ (A^{(0)} + \delta A^{(1)} + \mathcal{O}(\delta^2))^\top (P^{(0)} + \delta P^{(1)} + \mathcal{O}(\delta^2)) + C^\top C = 0, \end{aligned}$$

where we dropped the subscript (m, μ) for readability. By collecting terms associated with powers of δ , we obtain two Lyapunov equations determining $P^{(0)}$ and $P^{(1)}$:

$$P^{(0)}A^{(0)} + A^{(0)\top}P^{(0)} + C^\top C = 0, \quad (30a)$$

$$P^{(1)}A^{(0)} + A^{(0)\top}P^{(1)} + (P^{(0)}A^{(1)} + A^{(1)\top}P^{(0)}) = 0. \quad (30b)$$

By the same reasoning as used for equation (8), the first Lyapunov equation (30a) is feasible with a positive semidefinite $P^{(0)}$ satisfying $P^{(0)}v_0 = \mathbf{0}_{2n}$. The second Lyapunov equation (30b) is feasible by analogous arguments. Finally, by using (26) together with (28) and (29), we obtain

$$f(m + \delta\mu) = f_{(m,\mu)}^{(0)} + f_{(m,\mu)}^{(1)}\delta + \mathcal{O}(\delta^2),$$

where $f_{(m,\mu)}^{(0)} = f(m)$ and

$$f_{(m,\mu)}^{(1)} = \text{Trace} \left(2 B_{(m,\mu)}^{(1)\top} P_{(m,\mu)}^{(0)} B_{(m,\mu)}^{(0)} + B_{(m,\mu)}^{(0)\top} P_{(m,\mu)}^{(1)} B_{(m,\mu)}^{(0)} \right). \quad (31)$$

From (25), it follows that $\nabla_\mu f(m) = f_{(m,\mu)}^{(1)}$ as defined in (31), thereby implicitly establishing differentiability of $f(m)$.

This concludes the proof, as the algorithm computes each component of the gradient $\nabla f(m)$ by using the relation (24) with the special choice of $\mu = \mathbf{e}_i$ for $i \in \{1, \dots, n\}$. \square

3.5 The planning problem: economic allocation of resources

In this subsection, we focus on the planning problem of optimally allocating virtual inertia when economic reasons suggest that only a limited number of virtual inertia devices should be deployed (rather than at every grid bus). Since this problem is generally combinatorial, we solve a modified optimal allocation problem, where an additional ℓ_1 -regularization penalty is imposed, in order to promote a sparse solution [30].

The regularized optimal inertia allocation problem is then

$$\underset{P, m_i}{\text{minimize}} \quad J_\gamma(m, P) = \|G\|_2^2 + \gamma \|m - \underline{m}\|_1 \quad (32a)$$

$$\text{subject to} \quad \sum_{i=1}^n m_i \leq m_{\text{bdg}} \quad (32b)$$

$$\underline{m}_i \leq m_i \leq \bar{m}_i, \quad i \in \{1, \dots, n\} \quad (32c)$$

$$PA + A^\top P + C^\top C = 0, \quad Pv_0 = \mathbf{0}_{2n}, \quad (32d)$$

where $\gamma \geq 0$ trades off the sparsity penalty and the original objective function.

As in (32c) the allocations m_i are lower bounded by a positive \underline{m}_i , the objective (32a) can be rewritten as:

$$J_\gamma(m, P) = \text{Trace}(B^\top P B) + \sum_{i=1}^n \gamma (m_i - \underline{m}_i). \quad (33)$$

Observe that the regularization term in the cost (33) is linear and differentiable. Thus, problem (33) fits well into our

gradient computation algorithm, and a solution can be determined within the fold of Algorithm 1 by incorporating the penalty term. Likewise, our analytic results in Section 3.2 can be re-derived for the cost function (33). We highlight the utility of the performance-sparsity trade-off (33) in Section 4.

4 Case study: 12-Bus-Three-Region System

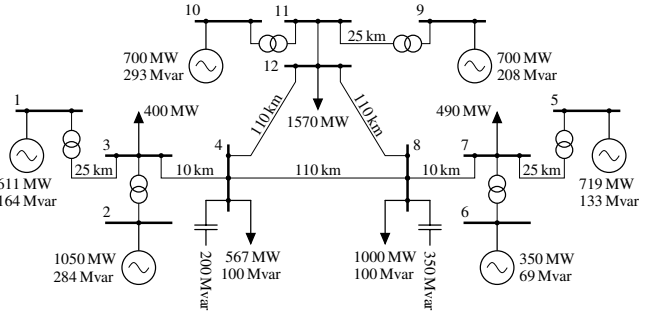


Figure 3: A 12 bus three-region test case adopted from [11, 24]. Transformer reactance 0.15 p.u., line impedance $(0.0001 + 0.001i)$ p.u./km.

In this section, we investigate a 12-bus case study illustrated in Figure 3. The system parameters are based on a modified two-area system from [24, Example 12.6] with an additional third area, as introduced in [11]. After Kron reduction of the passive load buses, we obtain a systems of 9 buses, corresponding to the nodes where inertia can be allocated.

We investigate this example computationally using Algorithm 1 to drive standard gradient-based optimization routines, while highlighting parallels to our analytic results. We analyze different parametric scenarios and compare the inertia allocation and the performance of the proposed numerical optimization (which is a locally optimal solution) with two plausible heuristics that one may deduce from the conclusions in [3, 11] and the special cases discussed following Theorem 3: namely the uniform allocation of the available budget, in the absence of capacity constraints, that is, $m_i = m_{\text{uni}} = m_{\text{bdg}}/n$; or the allocation of the maximum inertia allowed by the bus capacity constraints in the absence of a budget constraint, that is, $m = \bar{m}$ (which we set as $\bar{m}_i = 4\underline{m}_i$).

Uniform disturbance We first assume that the disturbance affects all nodes identically, $T = I_n/9$. In Figure 4 we consider the case where there are only capacity constraints at each bus, and we compare the different allocations vis-à-vis: the initial inertia \underline{m} , a locally optimal solution m^* , and the maximum inertia allocation \bar{m} . Figure 5 compares the results in the case where there is only a budget constraint on the total allocation. We compare the initial inertia \underline{m} , the locally optimal allocation m^* , and the uniform placement $m_i = m_{\text{uni}}$.

Localized disturbance We then consider the scenario where a localized disturbance affects a particular node, in this example, node 4 with $T = \text{diag}\{0, 0, 1, 0, 0, 0, 0, 0\}$. As in Figures 4 and 5, a comparison of the different inertial allocations and the performance values is presented in Figures 6 and 7 for the cases of capacity and budget constraints.

We draw the following conclusions from the above test cases – some of which are perhaps surprising and counterintuitive.

1. First, our locally optimal solution achieves the best performance among the different heuristics in all scenarios.
2. In the case of uniform disturbances with only capacity constraints on the individual buses (Figure 4), the optimal solution does not correspond to allocating the maximum possible inertia at every bus.
3. In the case of uniform disturbances with only the total budget constraint (Figure 5), the optimal solution is remarkably different from the uniform allocation of inertia at the different nodes.
4. In case of uniform disturbances, the performance improvement with respect to the initial allocation and the different heuristics is modest. This confirms the intuition developed for the two-area case (Section 3.3) regarding the flatness of the cost function.
5. In stark contrast is the case of a localized disturbance, where adding inertia dominantly to disturbed node is an optimal choice in comparison to heuristic placements. The latter is also in line with the results presented for the two-area case and the closed-form results in Theorem 3.
6. In the case of a localized disturbance, adding inertia to all undisturbed nodes may be detrimental for the performance, even for the same (maximal) allocation of inertia at the disturbed node, as shown in Figure 6.
7. In Figure 8, we show the optimal allocations for a convex combination of the angle and frequency penalties, that is, when the coherency performance metric (4) is modified as

$$\int_0^\infty (1 - \rho) \cdot \theta(t)^\top N \theta(t) + \rho \cdot \omega(t)^\top S \omega(t) dt,$$

where $\rho \in [0, 1]$. The optimal allocation appears more uniform across the network when penalizing only frequency violations, as suggested by Theorem 3 for the special case $(N, S) = (0, D)$.

8. The sparsity-promoting approach proposed in Section 3.5 is examined in Figure 9. For a uniform disturbance without a sparsity penalty, inertia is allocated at all nine buses of the network. For $\gamma = 6 \times 10^{-5}$ an allocation at only seven buses is optimal with hardly a 1.3% degradation in performance. For sparser allocations, the trade-off with performance becomes more relevant. The sparsity effect is significantly pronounced for localized disturbances. The optimal solution for $\gamma = 0$ for a localized disturbance at node 4, requires allocating inertia

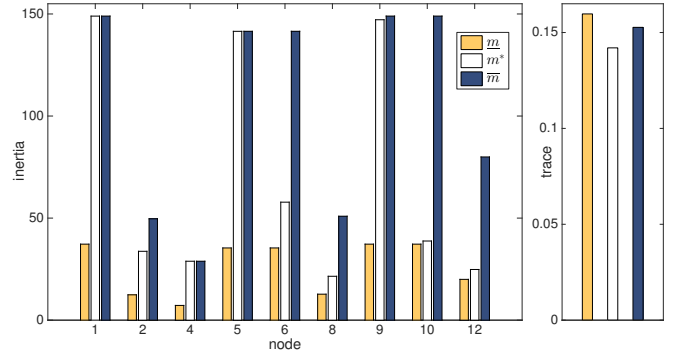


Figure 4: Optimal inertia allocation for a uniform disturbance subject to capacity constraints (10c).

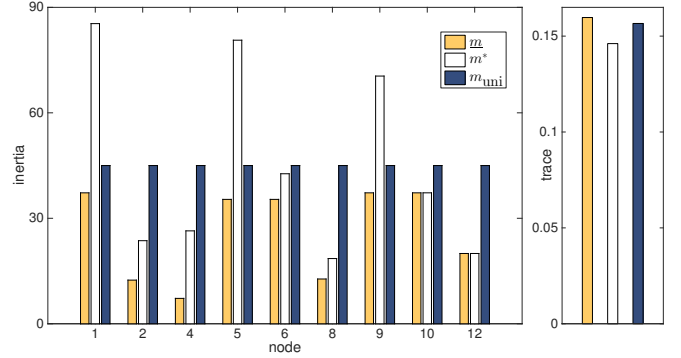


Figure 5: Optimal inertia allocation for a uniform disturbance subject to budget constraint (10b).

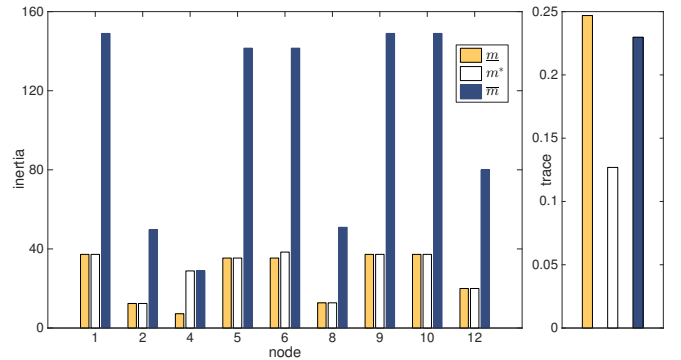


Figure 6: Optimal inertia allocation for a localized disturbance at node 4 subject to capacity constraints (10c).

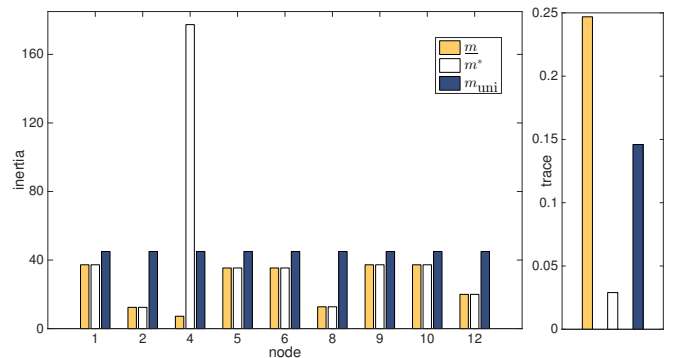


Figure 7: Optimal inertia allocation for a localized disturbance at node 4 subject to budget constraint (10b).

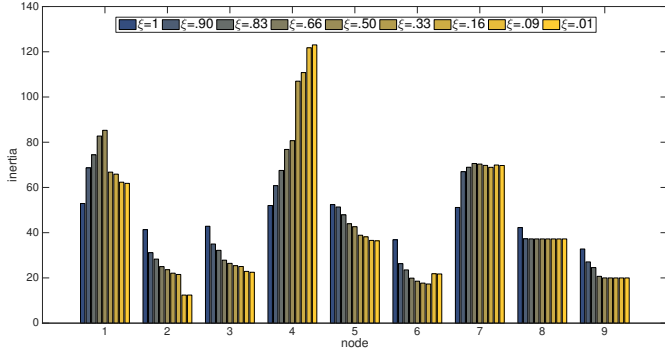


Figure 8: Optimal inertia allocation for a uniform disturbance, subject to budget constraints, and with a convex combination of penalties on angle differences N and frequency excursions S .

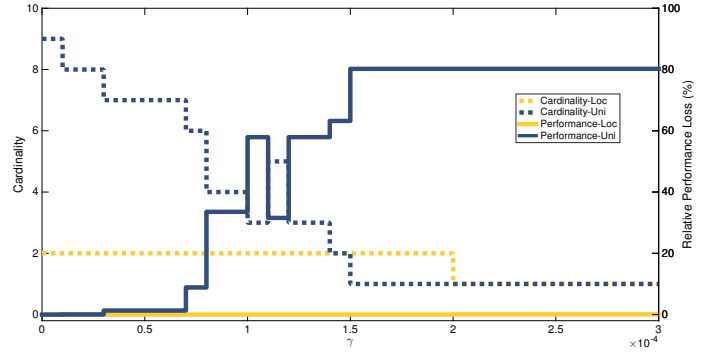


Figure 9: Relative performance loss (%) as a function of sparsity promoting penalty γ for (a) uniform disturbance, (b) localized disturbance at node 4 with capacity constraints. 0% performance loss corresponds to the optimal allocation, 100% performance loss corresponds to no additional inertia allocation.

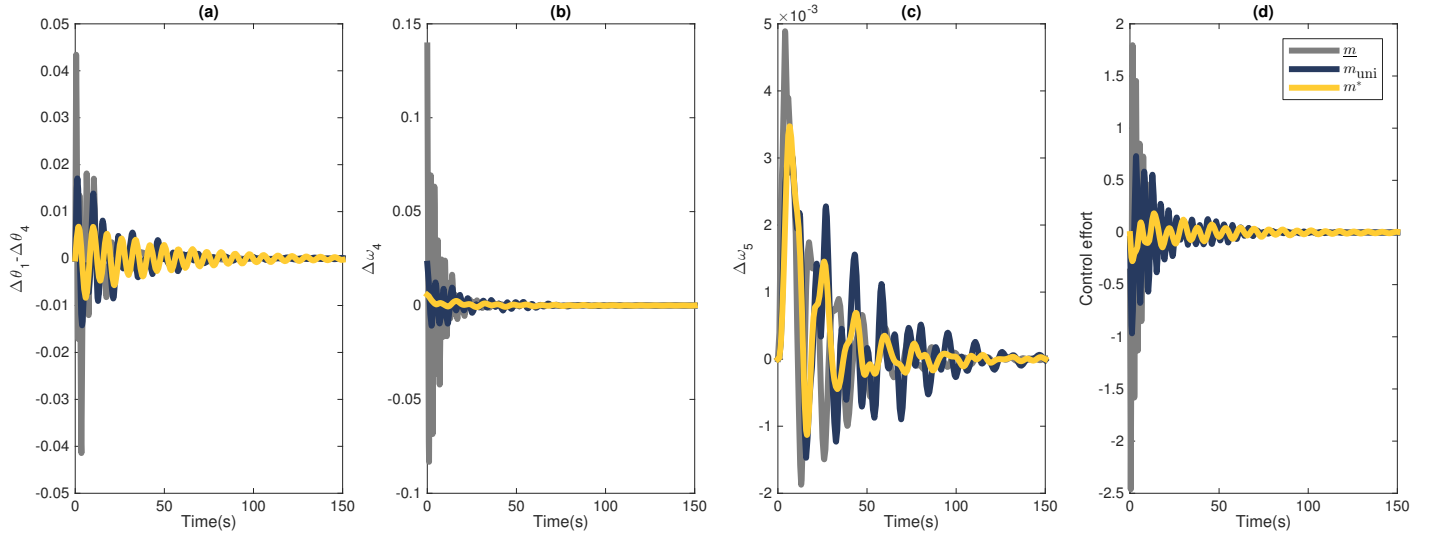


Figure 10: Time-domain simulations of angle differences, select frequencies, and control effort for a localized disturbance at node 4.

at buses (4, 6). However, for $\gamma = 2 \times 10^{-4}$, we observe an allocation of inertia only at bus 4 does not affect the performance significantly, while being preferable from an economic perspective.

9. Figure 10 shows the time domain responses to a localized impulse at node 4, modeling a post-fault condition. Subfigure (a) (respectively, (b)) detail the superior performance of an optimal inertia allocation with regards to the peak (overshoot) for angle differences (respectively, frequencies). Subfigure (c) displays the frequency response at node 5 of the system. Note that the scale of this plots is of order 10^{-3} rendering the deviations as potentially insignificant. Similar comments apply to other signals which are not displayed here. Finally subfigure (d) shows the control effort $m \cdot \ddot{\theta}_i$ expended by the virtual inertia emulation at the disturbed bus i . Perhaps surprisingly, observe that the optimal allocation $m = m^*$ requires the least control effort.

10. Figure 11 plots the eigenvalue spectrum for different inertia profiles. The case of no additional inertia allocation, $m = \underline{m}$, marginally outperforms with respect to both the best damping asymptote (most damped nonzero eigenvalues) as well as the best damping ratio (narrowest cone). This is the optimization criterion in [11]. As apparent from the time-domain plots in Figure 10, this case also leads to the worst time-domain performance (with respect to overshoots) compared to the optimal allocation $m = m^*$, which has slightly poorer damping asymptote and ratio. These observations reveal that the spectrum holds only partial information, and they strongly advocate the use of the \mathcal{H}_2 -norm as opposed to spectral performance metrics.

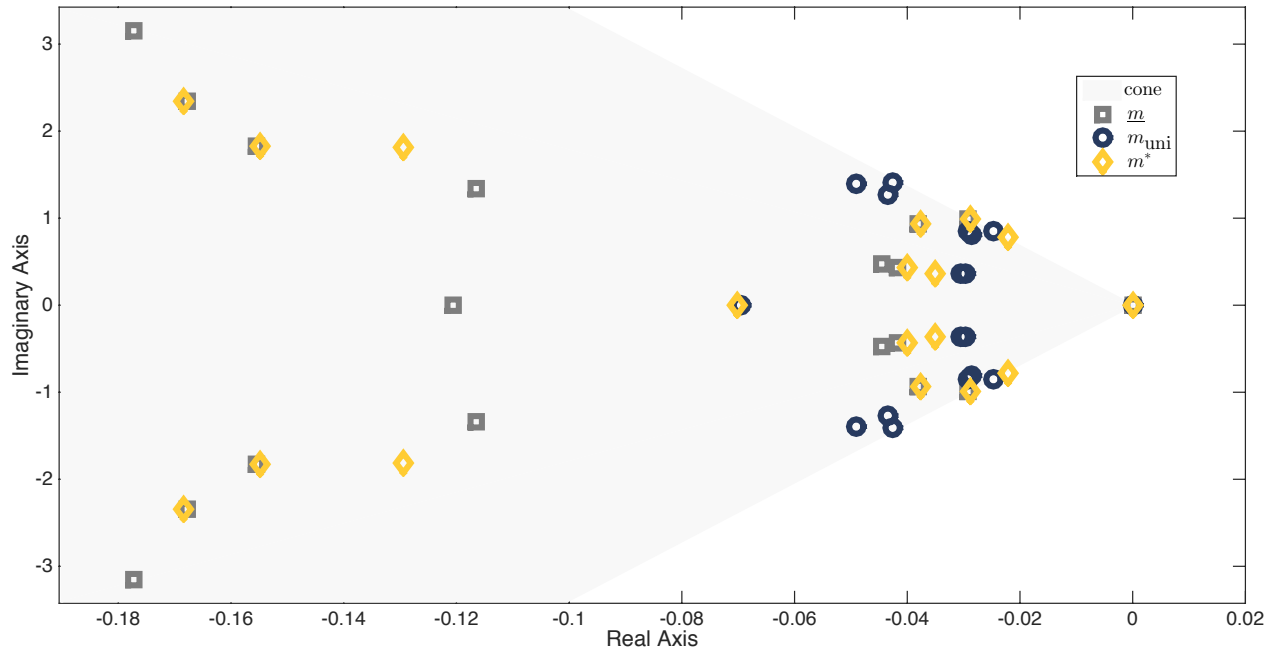


Figure 11: The eigenvalue spectrum of the state matrix A for different inertia profiles, where m^* has been optimized for a localized disturbance at node 4.

5 Conclusions

We considered the problem of placing virtual inertia in power grids based on an \mathcal{H}_2 norm performance metric reflecting network coherency. This formulation gives rise to a large-scale and non-convex optimization program. For certain cost functions, problem instances, and in the low-dimensional two-area case, we could derive closed-form solutions yielding some, possibly surprising insights. Next, we developed a computational approach based on an explicit gradient formulation and validated our results on a three-area network. Suitable time-domain simulations demonstrate the efficacy of our locally optimal inertia allocations over intuitive heuristics. We also examined the problem of allocating a finite number of virtual inertia units via a sparsity-promoting regularization. All of our results showcase that the optimal inertia allocation is strongly dependent on the location of disturbance.

Our computational and analytic results are well aligned and suggest insightful strategies for the optimal allocation of virtual inertia. We envision that these results find application in stabilizing low-inertia grids through strategically placed virtual inertia units. As part of our ongoing and future work, we also consider the extension to more detailed system models.

Acknowledgements

The authors wish to thank Mihailo Jovanovic, Andreas Ulbig, Theodor Borsche, Dominic Gross, and Ulrich Münz for their comments on the problem setup and analysis methods.

References

- [1] W. Winter, K. Elkington, G. Bareux, and J. Kostevc, "Pushing the limits: Europe's new grid: Innovative tools to combat transmission bottlenecks and reduced inertia," *Power and Energy Magazine, IEEE*, vol. 13, no. 1, pp. 60–74, Jan 2015.
- [2] M. Milligan, B. Frew, B. Kirby, M. Schuerger, K. Clark, D. Lew, P. Denholm, B. Zavadil, M. O'Malley, and B. Tsuchida, "Alternatives no more: Wind and solar power are mainstays of a clean, reliable, affordable grid," *Power and Energy Magazine, IEEE*, vol. 13, no. 6, pp. 78–87, 2015.
- [3] A. Ulbig, T. S. Borsche, and G. Andersson, "Impact of low rotational inertia on power system stability and operation," in *IFAC World Congress*, vol. 19, no. 1, 2014, pp. 7290–7297.
- [4] N. Soni, S. Doolla, and M. C. Chandorkar, "Improvement of transient response in microgrids using virtual inertia," *Power Delivery, IEEE Transactions on*, vol. 28, no. 3, pp. 1830–1838, 2013.
- [5] H. Bevrani, T. Ise, and Y. Miura, "Virtual synchronous generators: A survey and new perspectives," *International Journal of Electrical Power & Energy Systems*, vol. 54, pp. 244–254, 2014.
- [6] S. D'Arco and J. Suul, "Virtual synchronous machines – classification of implementations and analysis of equivalence to droop controllers for microgrids," in *PowerTech (POWERTECH), 2013 IEEE Grenoble*, June 2013, pp. 1–7.

- [7] J. Morren, S. W. H. De Haan, W. L. Kling, and J. A. Ferreira, "Wind turbines emulating inertia and supporting primary frequency control," *IEEE Transactions on Power Systems*, 21 (1), 2006.
- [8] M. Koller, T. Borsche, A. Ulbig, and G. Andersson, "Review of grid applications with the zurich 1 {MW} battery energy storage system," *Electric Power Systems Research*, vol. 120, pp. 128 – 135, 2015.
- [9] P. Ashton, C. Saunders, G. Taylor, A. Carter, and M. Bradley, "Inertia estimation of the gb power system using synchrophasor measurements," *Power Systems, IEEE Transactions on*, vol. 30, no. 2, pp. 701–709, March 2015.
- [10] E. Ela, V. Gevorgian, A. Tuohy, B. Kirby, M. Milligan, and M. O'Malley, "Market designs for the primary frequency response ancillary service – part i: Motivation and design," *Power Systems, IEEE Transactions on*, vol. 29, no. 1, pp. 421–431, 2014.
- [11] T. S. Borsche, T. Liu, and D. J. Hill, "Effects of rotational inertia on power system damping and frequency transients," in *Conference on Decision and Control*, 2015, to appear.
- [12] K. Zhou, J. C. Doyle, and K. Glover, *Robust and Optimal Control*. Prentice Hall, 1996.
- [13] E. Lovisari and S. Zampieri, "Performance metrics in the average consensus problem: a tutorial," *Annual Reviews in Control*, vol. 36, no. 1, pp. 26–41, 2012.
- [14] B. Bamieh, M. R. Jovanovic, P. Mitra, and S. Patterson, "Coherence in large-scale networks: Dimension-dependent limitations of local feedback," *IEEE Transactions on Automatic Control*, vol. 57, no. 9, pp. 2235–2249, 2012.
- [15] M. Fardad, F. Lin, and M. R. Jovanovic, "Design of optimal sparse interconnection graphs for synchronization of oscillator networks," *Automatic Control, IEEE Transactions on*, vol. 59, no. 9, pp. 2457–2462, 2014.
- [16] M. Fardad, X. Zhang, F. Lin, and M. R. Jovanović, "On the properties of optimal weak links in consensus networks," in *Proceedings of the 53rd IEEE Conference on Decision and Control*, Los Angeles, CA, 2014, pp. 2124–2129.
- [17] T. Summers, I. Shames, J. Lygeros, and F. Dörfler, "Topology design for optimal network coherence," in *European Control Conference*, 2015, Available at <http://arxiv.org/abs/1411.4884>. [Online]. Available: <http://arxiv.org/abs/1411.4884>
- [18] M. Siami and N. Motee, "Systemic measures for performance and robustness of large-scale interconnected dynamical networks," in *Decision and Control (CDC), 2014 IEEE 53rd Annual Conference on*. IEEE, 2014, pp. 5119–5124.
- [19] E. Sjödin, B. Bamieh, and D. F. Gayme, "The price of synchrony: Evaluating the resistive losses in synchronizing power networks," *IEEE Transactions on Control of Network Systems*, 2015, to appear.
- [20] F. Dörfler, M. R. Jovanovic, M. Chertkov, and F. Bullo, "Sparsity-promoting optimal wide-area control of power networks," *IEEE Transactions on Power Systems*, vol. 29, no. 5, pp. 2281–2291, September 2014.
- [21] X. Wu, F. Dörfler, and M. R. Jovanovic, "Input-output analysis and decentralized optimal control of inter-area oscillations in power systems," *IEEE Transactions on Power Systems*, February 2015, to appear.
- [22] F. Dörfler, J. W. Simpson-Porco, and F. Bullo, "Breaking the Hierarchy: Distributed Control & Economic Optimality in Microgrids," *IEEE Transactions on Control of Network Systems*, 2015, to appear.
- [23] P. W. Sauer and M. A. Pai, *Power System Dynamics and Stability*. Prentice Hall, 1998.
- [24] P. Kundur, *Power System Stability and Control*. McGraw-Hill, 1994.
- [25] F. Dörfler and F. Bullo, "Kron reduction of graphs with applications to electrical networks," *IEEE Transactions on Circuits and Systems I: Regular Papers*, vol. 60, no. 1, pp. 150–163, 2013.
- [26] Q.-C. Zhong and T. Hornik, *Control of Power Inverters in Renewable Energy and Smart Grid Integration*. Wiley-IEEE Press, 2013.
- [27] J. Schiffer, D. Zonetti, R. Ortega, A. Stankovic, T. Sezi, and J. Raisch, "Modeling of microgrids-from fundamental physics to phasors and voltage sources," *arXiv preprint arXiv:1505.00136*, 2015.
- [28] J. Schiffer, D. Goldin, J. Raisch, and T. Sezi, "Synchronization of droop-controlled autonomous microgrids with distributed rotational and electronic generation," in *IEEE Conf. on Decision and Control*, Florence, Italy, Dec. 2013, pp. 2334–2339.
- [29] D. P. Bertsekas, *Convex Optimization Algorithms*. Athena Scientific, 2015.
- [30] E. J. Candès, M. B. Wakin, and S. P. Boyd, "Enhancing sparsity by reweighted ℓ_1 minimization," *Journal of Fourier Analysis and Applications*, vol. 14, no. 5, pp. 877–905, 2008.